# DYNAMICS OF THE TRANSITION CORONA

SOPHIE MASSON[1,2], PATRICK MCCAULEY[3], LEON GOLUB[3], KATHARINE K. REEVES[3], AND EDWARD E. DELUCA[3]
[1] Space Weather Laboratory–NASA Goddard Space Flight Center, 8800 Greenbelt Road, Greenbelt, MD, USA; sophie.masson@nasa.gov
[2] Catholic University of America, 620 Michigan Avenue NE, Washington, DC, USA
[3] Harvard-Smithsonian Center for Astrophysics, 60 Garden Street, Cambridge, MA, USA

## ABSTRACT

Magnetic reconnection between the open and closed magnetic fields in the corona is believed to play a crucial role in the corona/heliosphere coupling. At large scale, the exchange of open/closed connectivity is expected to occur in pseudo-streamer (PS) structures. However, there is neither clear observational evidence of how such coupling occurs in PSs, nor evidence for how the magnetic reconnection evolves. Using a newly developed technique, we enhance the off-limb magnetic fine structures observed with the Atmospheric Imaging Assembly and identify a PS-like feature located close to the northern coronal hole. We first identify that the magnetic topology associated with the observation is a PS, null-point (NP) related topology bounded by the open field. By comparing the magnetic field configuration with the EUV emission regions, we determined that most of the magnetic flux associated with plasma emission are small loops below the PS basic NP and open field bounding the PS topology. In order to interpret the evolution of the PS, we referred to a three-dimensional MHD interchange reconnection modeling the exchange of connectivity between small closed loops and the open field. The observed PS fine structures follow the dynamics of the magnetic field before and after reconnecting at the NP obtained by the interchange model. Moreover, the pattern of the EUV plasma emission is the same as the shape of the expected plasma emission location derived from the simulation. These morphological and dynamical similarities between the PS observations and the results from the simulation strongly suggest that the evolution of the PS, and in particular the opening/closing of the field, occurs via interchange/slipping reconnection at the basic NP of the PS. Besides identifying the mechanism at work in the large-scale coupling between the open and closed fields, our results highlight that interchange reconnection in PSs is a gradual physical process that differs from the impulsive reconnection of the solar-jet model.

*Key words:* Sun: corona – Sun: magnetic fields – Sun: UV radiation

*Online-only material:* animations, color figures

## 1. INTRODUCTION

Understanding how the corona couples with the heliosphere is critical for making advances on the origin of the solar wind. Although it is generally acknowledged that the fast wind originates from coronal holes, the slow solar wind seems to originate from the boundaries between the open and closed fields. Among other properties (see review by Antiochos et al. 2012), the slow solar wind has the elemental composition of the closed corona (Zurbuchen et al. 2002), which contrasts with the photospheric elemental composition observed in the fast solar wind. In order to explain these composition properties, Wang et al. (2000) proposed that the slow wind comes from the opening of the closed Helmet streamer loops through reconnection at the boundary of the open/closed fields of the Helmet streamer, allowing the release of closed loop material into open flux. However, this model restricts the slow solar wind to the heliospheric current sheet (HCS) region and does not account for the latitudinal expansion over tens of degrees of the slow solar wind. The recent S-Web model by Antiochos et al. (2011), Titov et al. (2011), and Linker et al. (2011) completed this theory by showing that a web of separatrices/quasi-separatrix layers (QSLs), connecting the closed and the open fields, is located around the HCS and provides the environment for open/closed connectivity exchange at higher latitudes than the HCS.

The structures ensuring the transition between the open and closed fields in the corona are of two kinds. The Helmet streamer separates the open field of opposite polarity, while the pseudo-streamer (PS) separates the open field

of the same polarity and therefore includes a null point (NP) at the transition between the open and closed fields (Wang et al. 2007; Titov et al. 2012). In Helmet streamers, the release of material into the heliosphere may result from magnetic reconnection either along the open/closed separatrix surface or at the apex of the streamer, where the field is extended under the solar wind pressure (Wang et al. 2000). This latter process leads to the formation of plasma blobs that escape into the Heliosphere (Sheeley et al. 1997; Wang et al. 1998). For opening the field in a PS, it is commonly acknowledged that interchange reconnection occurs at the NP, exchanging the connectivity between the open and closed fields (Antiochos et al. 2002; Edmondson et al. 2009; Masson et al. 2012). While plasma blobs detaching from the streamer's apex are detected in white-light coronagraph images, the dynamics of PSs show a quasi-steady state without any distinguishable features above 2 solar radii (Wang et al. 2012). By nature, a PS's cusp is located lower in the corona and, consequently, the transition between the open and closed fields is not detected by coronagraphs, as is the case for streamers. However, several studies showed that the base of a PS formed by two closed lobes bounded by a diverging open field can be observed in the low corona at EUV wavelengths (Filippov et al. 2013; Seaton et al. 2013).

Even though interchange reconnection is expected in such PS configurations, there is no indication that interchange reconnection is indeed responsible for the observed PS signature or for the field opening. First, while interchange reconnection is usually attributed to a NP topology surrounded by the open
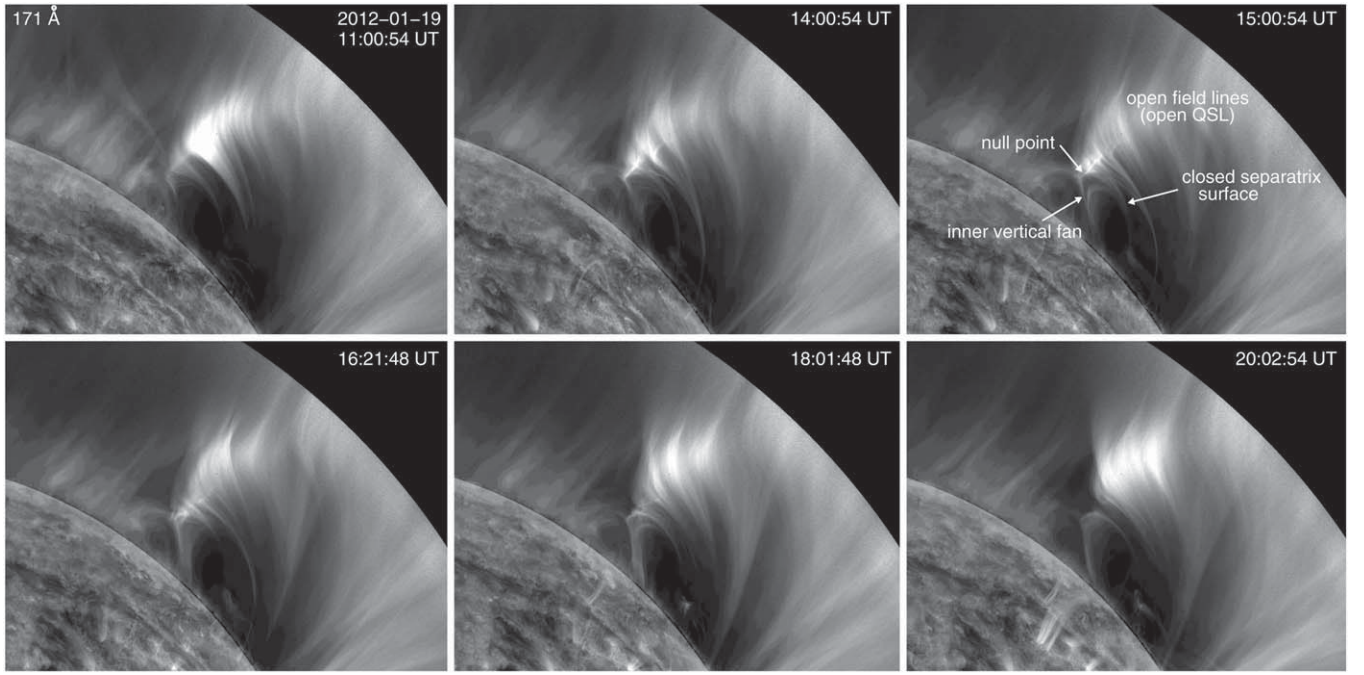
**Figure 1.** Temporal sequence showing the evolution of the emission at 171 Å observed by AIA/*SDO*. We distinguish the open and closed field lines and the null-point current sheet. In the top right panel we labeled these structures according to the pseudo-streamer topology described in Section 3.1.

(Animations of this figure are available in the online journal.)

field, in reality, PSs have a more complex topology formed by several NPs linked by separators (see Titov et al. 2012). Therefore, the dynamics of the reconnection coupling open and closed fields in PSs might not be as straightforward as it is for a single NP. Second, previous studies of interchange reconnection have mostly focused on explaining solar jets (Moreno-Insertis et al. 2008; Pariat et al. 2009). Therefore, those interchange models for jets lead to explosive dynamics that are consistent with jet observations (Cirtain et al. 2007), but they do not correspond to the gradual and quasi-steady evolution of the PS structures at high coronal altitudes (Wang et al. 2007).

In this article, we examine the dynamics of EUV observations of a PS-like structure identified in Atmospheric Imaging Assembly (AIA; Lemen et al. 2012) data. The high cadence and spatial resolution of AIA allow us to infer the dynamics of the coronal magnetic structures (Section 2). In Section 3, we present the topology related to the EUV PS and the reconnection regimes that can potentially take place in such PS configuration. In order to determine the mechanisms responsible for the PS activity, we first identify the magnetic configuration where EUV emission is observed (Section 4.1). Then, we use results from a three-dimensional (3D) MHD simulation of NP interchange reconnection to determine the reconnection regimes that may be at work in the PS open/closed coupling (Section 4.2). Finally, we conclude and discuss our results in Section 5.

## 2. EUV OBSERVATIONS OF PSEUDO-STREAMER WITH AIA

The observations reported here were taken on 2012 January 19 by the AIA instrument aboard the *Solar Dynamics Observatory* (*SDO*; Pesnell et al. 2012). We examine a streamer structure on the west limb, at the border of a northern coronal hole located between $35°-60°$ N and between $60° \geqslant 90°$ W. AIA records full-Sun images in seven extreme ultraviolet channels with a 12 s cadence and a resolution of $0''6$ pixel$^{-1}$. Of these, the

171 Å band is most suited to our model comparison because it best resolves the fine magnetic structures in the corona. This channel is dominated by Fe IX, with a characteristic temperature of $10^{5.8}$ (O'Dwyer et al. 2010).

To further enhance fine structure, we have processed the observations using a radial filter. This begins by summing the off-limb component of several images to increase signal-to-noise ratio. The corona beyond the disk is then divided into concentric rings, each of which is scaled as a function of its radius, average brightness, and intensity relative to neighboring rings. As such, flux is not conserved; the brightness of each pixel corresponds only to its intensity relative to other pixels of the same radius (see the SolarSoft routine <aia_rfilter> and http://aia.cfa.harvard.edu/rfilter.shtml for details). For this application, we have used 10 image sums, yielding images with total integration times of ∼20 s over two-minute periods. Figure 1 displays a set of six images between 11:00 UT and 21:00 UT, and two corresponding animations are available in the online journal. While the heated plasma is constrained by the magnetic field, the bright strands observed in AIA explicitly indicate the geometry and the directivity of the magnetic field.

In Figure 1, we observe that some of the strands are closed, forming two lobes enclosing a darker region, and some other strands are open and bound the two closed lobes. The shape of the open strands shows a diverging pattern, as do the fan-like structures identified in EUV wavelengths in the low corona (Habbal et al. 2011; Seaton et al. 2013). In addition, at the intersection of the closed and open flux, we notice a thin extended region that becomes brighter and thinner as the system evolves. According to numerical studies, such a structure could correspond to the current sheet forming at the sheared NP (Rickard & Titov 1996; Galsgaard et al. 2003; Masson et al. 2009; Pariat et al. 2009; Galsgaard & Pontin 2011).

While such EUV structures have been clearly identified to be related to a PS configuration, the short-term dynamics of those structures have never been observed. The high spatial resolution
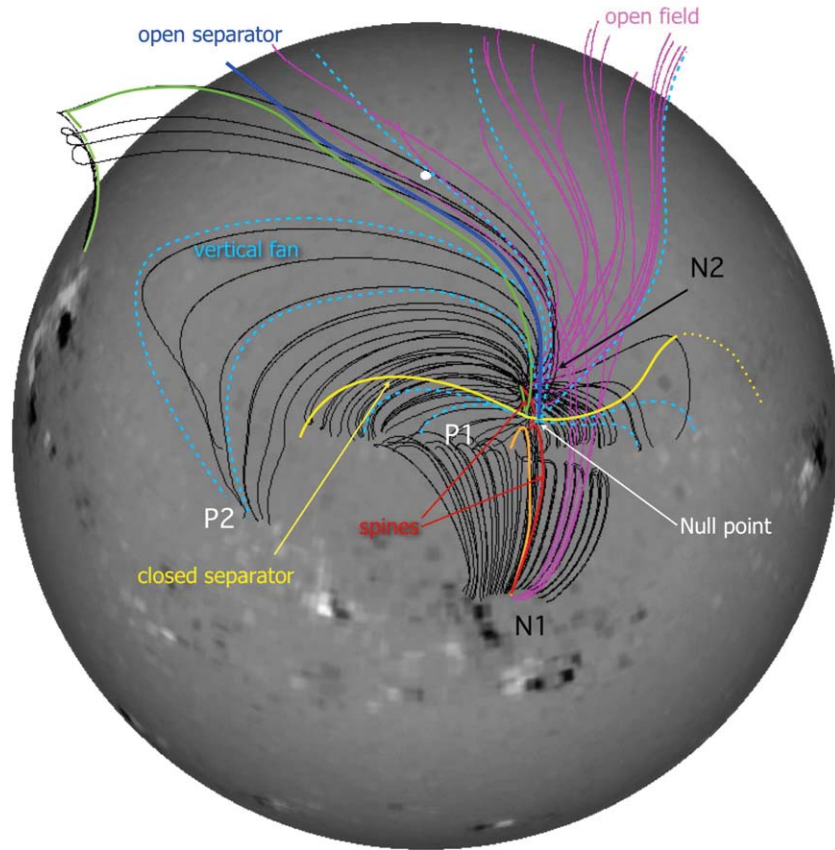
**Figure 2.** Topology of the pseudo-streamer from the PFSS extrapolation. The black field lines show the closed field lines whereas the pink field lines show the open field toward the interplanetary medium. The two red lines show the spines and the light blue dotted lines shows the vertical fan surface. The yellow line that passes through the null point shows the closed separator, while the dark blue plain line corresponds to an open separator. The green and the orange field lines show the large and small closed loops, respectively.

(A color version of this figure is available in the online journal.)

and high time cadence of AIA allow us to identify individual strands and to study their dynamics, providing the evolution of the reconnecting magnetic flux tubes. In the AIA observations, the general pattern of the event does not change drastically during the entire event, but the strands are highly dynamic (see the online material and Section 4.2.1 for details). According to Wang et al. (2007), PS structures observed in the EUV corona should be the result of magnetic reconnection at the cusp of the PS, i.e., at the NP, between the open and the closed field.

## 3. PSEUDO-STREAMER TOPOLOGY AND DYNAMICS

### 3.1. Magnetic Field Extrapolation

On the Carrington map CR2119 observed by HMI/*SDO* (Schou et al. 2012), the photospheric magnetic field related to the AIA observations lies between 35°–70°N and 70°–110°W of solar center at 12:00 UT on 2012 January 19. It includes the negative polarity of the north pole, one positive polarity from the trailing polarity of a western decayed active region, and one negative polarity corresponding to the leading polarity of a following decayed active region. We perform a Potential Field Source Surface (PFSS) extrapolation (Altschuler & Newkirk 1969) using the SolarSoft routines (Schrijver & De Rosa 2003) and determine the large-scale magnetic topology. Though the PFSS model cannot reproduce the exact magnetic configuration of the corona, it provides a robust method to obtain a reasonable approximation of the global magnetic topology (Brown & Priest 2001).

Figure 2 shows the magnetic field computed from the PFSS model. The black and pink field lines indicate the closed and open fields, respectively. The closed flux domain can be divided in two categories: small loops (e.g., orange line) connecting the southern (N1) and the northern (N2) negative polarities to the middle positive polarity (P1), and large loops (e.g., green line) connecting the N1 and N2 polarities to some eastern positive polarities (P2). Those large closed loops extend up to the source surface and are therefore part of a streamer configuration. For clarity, the large loops connecting N1 to P2 are not plotted on the Figure 2, but some of them are plotted on Figure 3. To the west of the central polarity, the closed flux is confined below open fluxes. Since the fluxes lie at low altitude and are located behind the limb for the AIA field of view, none of them are shown in Figure 2. Two open magnetic field regions (pink lines) are, respectively, located north and south of, rather than surrounding, the small closed magnetic flux. In P1 (middle positive polarity), the magnetic connectivity footprints of the low height closed field diverge. The global distribution of the magnetic field is very similar to the topology of one of the PSs described by Titov et al. (2012, see their Figures 8 and 9).

Even though the PFSS routines do not provide topological analysis, the magnetic field connectivity distribution can be used to derive the main topological elements. In Figure 2, we draw the separatrices and separators that should be present in a PS topology. We estimate the basic NP location in the region where the open and the closed fields converge. By plotting field lines
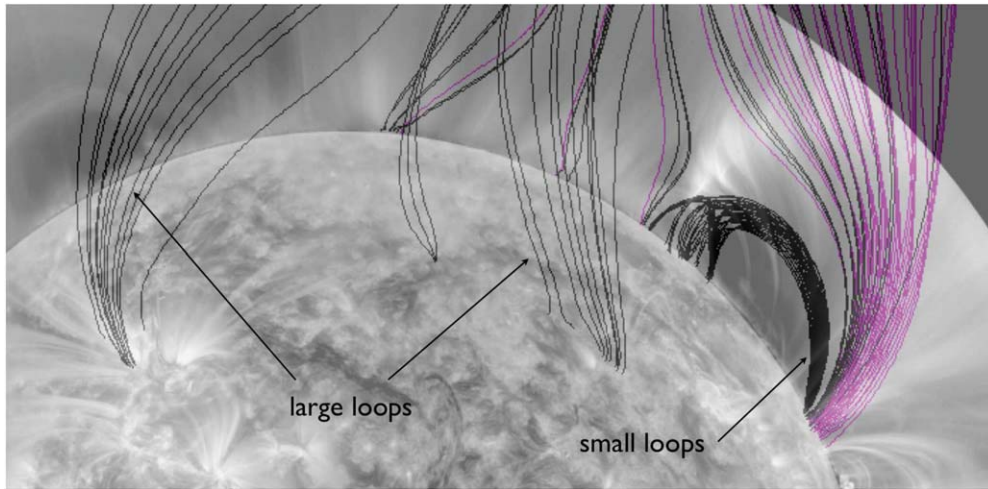
3

**Figure 3.** Sample of the open and closed field lines passing close to the null point overplotted on the AIA observations. The EUV emissions are located along the closed separatrix surface and the open field. No EUV emission is observed where the large closed loops are anchored.

(A color version of this figure is available in the online journal.)

passing in the vicinity of the NP, we determine its approximative location at $r \simeq 1.1\,R_\odot$ ($47°-52°.5\,N$, $95°-105°\,W$). From this basic NP emanates a vertical fan surface (or separatrix curtain), shown by the light blue dotted lines, and two spine lines (in red) connecting the two edging negative polarities (N1 and N2). Part of the fan surface is open, connected to the source-surface null line, and part of it is closed, anchored to the photosphere in P2 and P1. Thus, there is a jump in the connectivity mapping of the vertical fan from the open to closed flux domain, delimited by an open separator denoted by a dark blue line (Figure 2). This connects the basic NP and a source surface Y-point located at the cusp of the streamer. A closed separatrix surface, including the spines, encloses the small loops and separates them from the large loops connected to the P2 polarities. A closed separator line (yellow), passing through the basic NP, is present at the intersection of this closed separatrix surface and the vertical fan (see Titov et al. 2012 for details). The extremities of this closed separator can either be connected to NPs (a true NP–NP separator) or bald-patches (BPs; a NP–BP separator). By plotting a group of field lines in the vicinity of the eastern and western extremities of the closed separator of the PS topology, we determine that the field distributions are consistent with NPs and not bald patches. However, the quality of a PFSS extrapolation using synoptic maps is too low to unambiguously reach a firm conclusion on the small scale details of the magnetic topology.

In addition to the PS separatrices, QSLs are present in the domain (Antiochos et al. 2011; Titov et al. 2011, 2012) as for a singular NP topology (Masson et al. 2009, 2012). A QSL defines a region of strong gradients of connectivity (Priest & Démoulin 1995). Some of them surround the separatrix lines and surfaces (e.g., around the closed separatrix surface), and others are present by themselves (e.g., the open QSL formed by open diverging field). QSLs are a preferential site for the current formation. Finite-width thin current sheets develop and field lines exchange their connectivity continuously between neighboring field lines (Priest et al. 2003; Démoulin 2006; Aulanier et al. 2006). The presence of QSLs affect the dynamics of the reconnection during the event and therefore impact the evolution of reconnection signatures (e.g., Aulanier et al. 2007; Masson et al. 2009).

### 3.2. Magnetic Reconnection for Opening the Magnetic Field

The magnetic topology defines the connectivity of the magnetic field and therefore can be used to predict the global evolution of the magnetic field resulting from reconnection (Démoulin et al. 1994; Mandrini et al. 1997; Masson et al. 2009; Reid et al. 2012). We use the topology to determine where reconnection should occur and which magnetic fluxes should be involved. According to the PS magnetic field configuration, the closed flux can be opened in two different ways.

First, the basic NP delimits the open field and the small closed loops confined below the closed separatrix surface. When magnetic reconnection occurs at such a null, the closed field loops and the open field exchange their connectivity. This process is the standard interchange reconnection, extensively studied for a regular NP topology (Pariat et al. 2009; Edmondson et al. 2010; Linker et al. 2011; Masson et al. 2012), which induces the opening of the closed corona that releases mass and energy into the heliosphere. In the present case, interchange reconnection exchanges the connectivity of the small orange loop with the northern pink open field line rooted in N2 (see Figure 2). The initially closed orange line opens and joins the southern open flux (N1). The flux exchange also works the other way, with the northern small closed loops (P1–N2) reconnecting with the southern open field (N1).

The second scenario relies on the association of two reconnection episodes. In addition to the open field and the small closed field, the large loops also converge toward the NP (e.g., green line on Figure 2). Thus, reconnection between the large green and the small orange closed loops occurs at the NP. The initial large green loop closes down below the closed separatrix surface, forming a new small loop connecting the N2 and P1 polarities. The small orange loop jumps outside of the closed separatrix surface and forms a new large loop connecting the N1 and P2 polarities. While it results in a flux exchange across the vertical fan surface and the closed separatrix surface, it does not open the magnetic field. To do so, the newly reconnected large loop will open through a classical wind pressure opening or through magnetic reconnection along the open separator. Note that while magnetic reconnection at a closed separator has been studied (Parnell et al. 2010), magnetic reconnection

along an open separator has not. To our knowledge, there is no theoretical work that can help us to determine how magnetic reconnection proceeds along an open separator.

In addition to the regular interchange reconnection regime, the presence of QSLs surrounding separatrices affects the dynamics of the reconnection signatures during the event. Indeed, a slipping reconnection regime corresponds to a continuous reconnection between neighboring field lines and may be a source of continuous energy release (Aulanier et al. 2007; Baker et al. 2009; Reid et al. 2012; van Driel-Gesztelyi et al. 2012). Thus, this aspect cannot be ignored and the importance of QSL-reconnection for understanding the dynamics of the corona has been demonstrated for flares (Masson et al. 2009) and coronal mass ejections (Savcheva et al. 2012).

## 4. INTERPRETATION OF THE AIA OBSERVATIONS

### 4.1. Magnetic Structures Related to the EUV Emission

During magnetic reconnection, the energy release leads to heating episodes. Although very hot plasma can be observed during flares, the comparatively gentle and continuous reconnection process suggested by the gradual evolution of the EUV structures (Section 2) may only heat the plasma to lower temperatures of $\simeq 1$ MK. The plasma distributed along the reconnected field then cools and becomes visible in the 171 Å channel, which is sensitive to material at $\log(T) \sim 5.8$ K.

By comparing the magnetic field distribution with the location of the EUV emission from AIA observations, we determine the magnetic flux associated with the emitting plasma and therefore identify the magnetic field that have reconnected. To do so, we select field lines that pass close to the NP, where reconnection should occur, leading to energy release and probably heating episodes. On Figure 3, we over plotted these field lines on the AIA image at 15:28 UT, using the same color code than on Figure 2. The PFSS model allows us to determine the geometry of the field, but it cannot reproduce the exact magnetic configuration. First, the use of a potential field approximation does not contain currents. However, the field is evolving (as suggested by the dynamics of the bright AIA structures) and is, by definition, not potential. Second, the PFSS extrapolation is performed using a synoptic map, and the input photospheric magnetic field has been measured three days before the event when the region was at the disk center. The coronal activity and the photospheric motions have therefore changed the magnetic field distribution, but the global topology resulting from the large scale photospheric magnetic field is expected to be similar.

Even though the match is not perfect, we can still identify the magnetic flux associated with the EUV structures. The small loops are related to the bright closed structures confining a dark cavity, which we identified as a closed magnetic flux below the NP in the AIA observations. The open flux and the large loops anchored in N1 and N2 polarities are localized where the AIA open bright strands are observed. Furthermore, the NP location is close to the thin and intense bright elongated spot (see Section 2), supporting that the bright sheet corresponds to the NP current sheet.

The association between the EUV structures and the magnetic fluxes, as well as the NP current sheet, provides a consistent picture supporting that the bright EUV structures are at least partially caused by NP reconnection between closed flux below the null and the flux outside of it. As we described in Section 3.2, the opening can be achieved through a direct interchange reconnection, but also through a two step process which first

implies closed/closed reconnection between small and large loops, followed by an open/closed reconnection along the open separator.

In order to observe an increase of plasma emission, magnetic flux tubes have to be denser than their surrounding medium. Magnetic reconnection provides mechanisms that can trigger the filling of loops by plasma material (see Baker et al. 2009, references therein), such as chromospheric evaporation (Del Zanna 2008) and rarefaction wave driven by interchange reconnection between tenuous open and dense closed magnetic flux (Bradshaw et al. 2011). Whatever the process is, the time needed to fill a coronal loop is on the order of tens of minutes at most (Reeves et al. 2007). This is much shorter than the duration of the whole event, which lasts several hours. Therefore, if closed/closed reconnection occurs between the large and small loops, we expect to observe plasma emission all along the new reconnected loops anchored in P2 polarity, rather than only in the region co-spatial with the open flux. On Figure 3, as well as in animations 1 and 2, it clearly appears that no EUV emission is observed along the large closed field, suggesting that the AIA bright open strands are related to the open flux. Thus, EUV emission is mostly distributed along the closed flux below the NP and the open flux, suggesting that interchange reconnection between open and closed flux contributes significantly to the dynamics of the PS.

### 4.2. A 3D Model of Interchange Reconnection

In the following, we present the results of a 3D MHD simulation from Masson et al. (2012), hereafter M12, of an interchange reconnection in order to determine whether such open/closed reconnection can explain the observational conjectures in the previous section. Although this modeling is based on a NP, the PS topology has the same topological objects involved in NP interchange reconnection: the NP, the closed separatrix surface, and the open QSLs. By comparing the numerical results for a single NP topology and the PS observations, we expect to provide some clues for understanding the dynamics of the event. We are aware that the dynamics of reconnection for NPs and PSs should not be exactly the same, but we believe that the interchange at the NP should behave quite similarly. Besides, to our knowledge, there are no studies of the dynamics in PSs, and the 3D NP reconnection model is the most sophisticated model that we have to simulate interchange reconnection at a NP.

For our particular example, as we suggested in Section 4.1, NP reconnection between the open and closed fields seems to be predominant and single NP dynamics may suffice to capture the essential aspects of the open/closed coupling PS dynamics.

#### 4.2.1. Dynamics of the Magnetic Field

The 3D MHD simulation of M12 modeled an asymmetric NP topology, with a dome-like fan surface surrounded by an open diverging magnetic field, and studied the dynamics of interchange reconnection (see M12 for details).

The initial atmosphere is stratified, obeying hydrostatic equilibrium, and the temperature, gravity, and density profiles are adjusted to obtain a solar-like regime: $\beta$ is lower than 1 in the corona except at the NP where $\beta$ becomes greater than 1. In order to emulate the physics of the solar corona, the top and side boundaries of the numerical box are open, whereas the photospheric boundary is reflecting and line-tied. The system is forced by applying a sub-Alfvénic photospheric velocity flow, which moves the positive polarity toward negative $y$ in the area
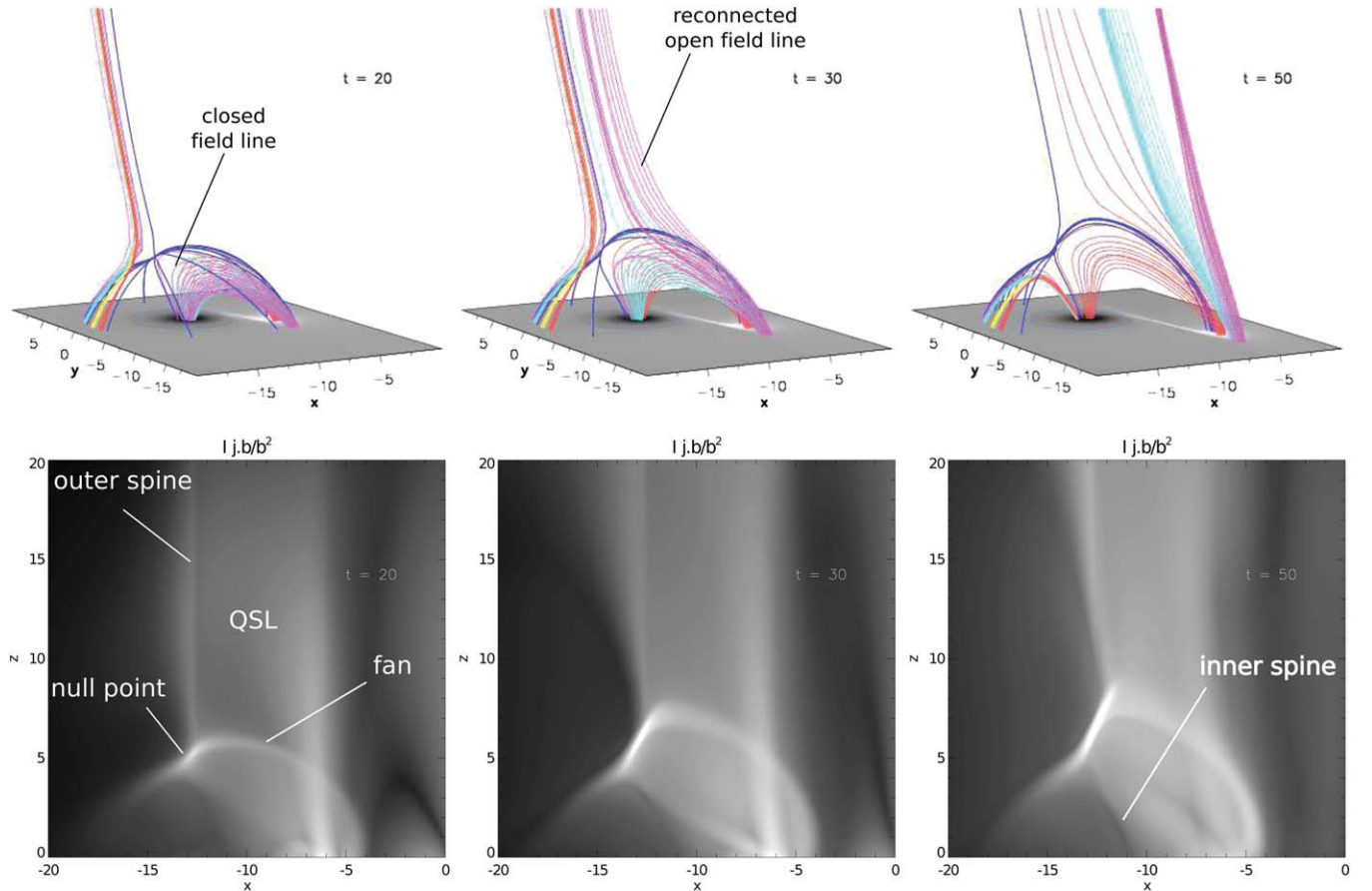
**Figure 4.** Results of the M12 simulation. Top row: evolution of the magnetic field lines during the interchange reconnection process. The grayscale code at the bottom boundary represents the vertical component of the magnetic field, and white and black show the positive and negative values, respectively. The dark blue field lines denote the fan and spine separatrix field lines and the groups of colored field lines (pink, red, yellow, light blue) display the open and the closed field lines that reconnect at the null point. Bottom row: temporal series of the 2D map of the integrated value of $\alpha^{0.33}$. The grayscale coding is black for $\alpha = 0$ and white for $\alpha = 2.34$).

(An animation and a color version of this figure are available in the online journal.)

of $x \in [-7, 3]$ and $y \in [10, -30]$, where a part of the fan is rooted.

This flow shears only part of the closed dome-like fan surface, increasing the asymmetry of the NP topology along the $y$-direction and leading to the extension of the open QSL-halo around the spine (Figure 5 in M12). It also leads to the bulging of field lines that compress the separatrices and a region of overdensity forms along the separatrices (Figures 4 and 2 in M12). Moreover, it induces a compression of the NP and misaligns the inner and the outer spine. Magnetic reconnection is expected to occur at the NP in order to bring the spines back into alignment (Rickard & Titov 1996; Antiochos et al. 2002; Galsgaard et al. 2003).

In order to determine the dynamics of magnetic reconnection, M12 plotted field lines from footpoints fixed in the advected positive polarity, integrated them up to their conjugate footpoints, and followed the evolution of the connectivities during the simulation. The top row of Figure 4 shows the evolution at three different times during the simulation. Initially, three groups of colored field lines have been plotted closed below the fan, and four groups of colored field lines open into the corona. The field lines are plotted from fixed footpoints. Following the connectivities of the conjugate footpoints of those field lines, M12 shows that magnetic reconnection occurs at the NP through interchange reconnection. The initially closed and open magnetic field lines exchange their connectivity and, respectively, open

into the corona and close down below the fan surface. In addition, the field lines show an apparent slipping motion before and after the NP interchange reconnection. These dynamics result from the slipping reconnection regime across the open QSLs that surround the fan-spine topology (Masson et al. 2012; see online material, animation 3).

The AIA observations show a two-dimensional (2D) projected evolution of a purely 3D phenomenon. It is therefore difficult to accurately follow the dynamics of the bright structures. We note that some initially closed field lines grow and approach the closed separatrix surface before disappearing (see animation 1). Meanwhile, there are also loops on the upper side of the NP that collapse into the null (animation 1 and 2). Around 14:00–15:00 UT there are loops underneath the null that shrink down, moving in the opposite sense of the loop pointed to in animation 1. Combined with line of sight effects, these field line motions are consistent with the dynamics of the interchange reconnection of M12. The initially closed field lines bulge and slip toward the NP, then reconnect at the NP and open in the corona. Furthermore, the open flux tubes move away from the NP area and show an apparent slipping motion (see animation 2). Such motions of the strands may correspond to the apparent motion of open field lines induced by the continuous reconnection across the open QSL (diverging open magnetic field), as suggested previously by Aulanier et al. (2007) for soft X-ray emission.

The dynamics of the fine structures observed with AIA show some strong similarities with the dynamics of the magnetic field derived from the M12 simulation (animation 3). Although the dynamics of the interchange reconnection in a simple NP topology cannot reproduce the full dynamics of the PS evolution, it provides some elements to understand it. Thus, the hybrid regime combining NP-interchange and slipping reconnection seems to reproduce the dynamics of the magnetic field derived from the EUV strands. This scenario leads us to propose that such an interchange/slipping regime may be responsible for the closed/open coupling leading to the energy release into the heliosphere.

### 4.2.2. Morphology of the Plasma Emission Regions

In order to support our interpretation of the mechanism powering the PS observation, we verify that such NP-interchange/slipping reconnection in an asymmetric NP topology can produce radiative signatures of reconnection similar to the PS observation. The numerical model of M12 focuses on the magnetic field dynamics but does not properly treat the plasma response. In the continuity equation, a nonphysical explicit diffusive term, which smooths the gradients, has been added. This term helps to stabilize the computation by avoiding cavitation or shock formation. In addition, the energy equation is reduced to the adiabatic temperature equation, to which a nonphysical explicit diffusive term has also been added for gradient smoothing. Therefore, the plasma is only heated by adiabatic effects and cools down via the diffusive term. Any other heating or cooling processes (e.g., Joule dissipation or radiation losses) are not included in the simulation. Since the density and temperature evolution do not reflect a correct plasma response (Section 4.2), we cannot generate synthetic images of the emission (Reeves et al. 2010) for comparison with the AIA observations.

Instead, we propose to use the current density distribution from the M12 simulation to determine where magnetic reconnection occurs. Given that the reconnection occurs continuously over several hours, we can estimate the location of cooling plasma that would be observed by the AIA 171 Å channel along the reconnected field. Intense currents are expected to be localized around the NP and along the separatrices, but also along the QSLs (Aulanier et al. 2006). In order to increase the contrast of regions where strong currents are expected, we use $\alpha = \mathbf{j}.\mathbf{b}/b^2$. This quantity is less dependent on the magnetic field magnitude but takes into account the orientation of the currents with respect to the field. Current sheets in the regions of weak magnetic field and strong magnetic gradient distributed on a coarse grid, e.g., the open QSL surrounding the outer spine, are highlighted by $\alpha$. According to the magnetic field distribution (Figure 3), the line of sight of the AIA observations aligns with the direction of the longitudinal extension axis of the closed flux. In order to be consistent with the AIA observations, which are integrated along the line-of-sight, we integrate the $\alpha$ parameter along the $y$ axis (extension axis of the closed flux in M12) from the boundary $y = -30$ to the $(x,z)$-plane at $y = 0$. This integration range avoids the part of the QSL located between $y = 0$ and $y = 30$, which results from the symmetry of the system (see M12).

The bottom row of Figure 4 shows the 2D maps of the integrated value of $\alpha$ at three different times. First, we identify the magnetic structures associated with the $\alpha$ structures. The brightest region indicated on this 2D $\alpha$-map corresponds to the current sheet located around the NP. The arc-shaped white

structure corresponds to the fan separatrix (delimiting the open and the closed magnetic field). Around $x = -15$ to $x = -10$, the black line embedded in the white halo corresponds to the inner and the outer spines (refer to labels in Figure 4). Finally, the extended white halo structure covering the area between $x \in [-15; -5]$ and $y \in [0; 20]$ is co-spatial with the reconnected open field lines belonging to the QSL.

Even though the intensity of the integrated-$\alpha$ does not reproduce the emission, it shows the location where energy release is expected and where plasma emission may be found. Previous studies have already shown an excellent association between the current density from simulations and the hot plasma emission at different wavelengths (e.g., Delannée et al. 2008; Aulanier et al. 2010; Savcheva et al. 2012). Comparing the AIA images and the synthetic $\alpha$-map, we notice that the emitting regions in AIA display the same patterns as the structures in the 2D-$\alpha$ map. We indeed find the thin and bright region at the null location, the arc-shaped white structures for the closed field and separatrix surface, and the extended bright open structure related to the open QSL. Similarly, the bright structure dividing the closed separatrix in two is also present in the $\alpha$-map and the AIA observations. We also note that the bright structure related to the NP on the observations (top middle and right panels of Figure 4) and on the $\alpha$-map (bottom row of Figure 4) becomes thinner and more intense as time goes on. Thus, the PS EUV emission shows the same reconnection signatures as the interchange reconnection in a single asymmetric NP topology. Those similarities strongly support our interpretation that the NP-interchange and slipping reconnection regimes are responsible for the PS dynamics observed with AIA.

## 5. CONCLUSION AND DISCUSSION

We explored the dynamics of a PS structure observed by AIA and suggested what mechanisms are at work by combining the magnetic topology of the event and a 3D MHD model of interchange reconnection from Masson et al. (2012), hereafter M12. The AIA 171 Å observations presented in this paper occurred on 2012 January 19 and correspond to an EUV PS. By applying a radial filter, we showed that the fine structures that trace magnetic fluxes are highly dynamic, while the global PS structure is more of a quasi-steady type (Section 2). Using the PFSS extrapolation, we showed that the magnetic configuration related to the AIA observations is a PS topology as defined by Titov et al. (2012). It is now well accepted that the dynamics of magnetic reconnection and the resulting radiative signatures are defined by the topology (Masson et al. 2009; Reid et al. 2012; Sun et al. 2013). For coronal field opening in a PS topology, interchange reconnection occurs at the NP either between the small loops and the open field or between small and large loops followed by reconnection along the open separator with the open field (Section 3.1). By comparing the location of the AIA/EUV structures and the magnetic field distribution from the PFSS extrapolation, we showed that interchange reconnection at the NP between closed and open field seems a plausible explanation of the PS observations.

The PS and NP topology are different, but both have a basic NP where interchange reconnection can occur between open and closed field. We expect to observe a behavior very similar to the NP topology given the observed PS topology. First, we showed that the dynamics of the open and closed magnetic field in the M12 interchange/slipping reconnection model is very similar to the dynamics of the white EUV strands in the AIA observations (Section 4.1). Second, we found that the distribution of plasma

emission expected by the M12 model has a shape very similar to the PS observation, showing that single NP reconnection, as in M12, can reproduce the observational signature of a PS (Section 4.2).

The location of the EUV emission, the similarities of the magnetic field dynamics, and the morphology of the radiative signatures are all pointing to the same conclusion: the PS observations result from the interchange/slipping reconnection at the basic PS NP. It is important to mention that the second scenario (see Section 3.2) involving magnetic reconnection at the open separator cannot be ruled out. It may also be involved in the dynamics of the PS, but it does not seem to dominate this particular event. Additional investigations into the dynamics of magnetic reconnection in a PS topology are needed to confirm the role of interchange reconnection at a basic NP, to determine the additional reconnection regime involved, and to establish how they affect the dynamics. Nonetheless, this study offers the first observational evidence for interchange reconnection occurring in a PS structure, where the open and closed fields are coupled through reconnection, leading to energy and mass transfer from the corona into the heliosphere. In addition, the M12 model deduces that the open white strands (see Figure 1) result from the QSL-reconnection, implying a continuous release of energy that can generate plasma emission lasting for several hours (see Baker et al. 2009 for details). This potentially explains why the open fluxes remained bright all along the event, rather than fading gradually after the NP reconnection. Note that the scaling applied to the model (Section 4.2) and the observations (Section 2) enhances the faint structures at high coronal height. This differential method used to produce the AIA images shown here allows us to better visualize the QSL structures in the corona.

One interesting characteristic of the M12 model is that the interchange reconnection is a gradual process, as in Edmondson et al. (2009), which is consistent with the dynamics of the observed PS that lasted for several hours without any drastic changes (see Seaton et al. 2013). According to Wang et al. (2000), PS configurations store and gradually release the energy over several hours and maybe days. Such behavior contrasts the explosive nature of solar jets (Cirtain et al. 2007) also caused by interchange reconnection at a single NP (Pariat et al. 2009). Even though both types of events are caused by interchange reconnection at NP, their dynamics result from two distinct reconnection regimes. Therefore, the explosive interchange solar-jet model cannot be applied to model reconnection dynamics in the large scale PS.

Although the exact role of the interchange reconnection in the origin of the solar wind is still under debate (see, e.g., Wang et al. 2012), it is very likely that this process is essential to releasing mass and energy into the heliosphere and that it somehow contributes to the solar wind generation. In agreement with Antiochos et al. (2011) and Titov et al. (2011), the global topology of the solar coronal magnetic field displays a web of similar PS topologies delimiting the open and closed magnetic field. This web of (quasi-)separatrices provides the environment for opening the closed coronal field through interchange reconnection all around the Sun. Moreover, Seaton et al. (2013) showed that the fan-like structures, with a cusp located low in the corona (below 2 solar radii), are present over the entire solar cycle. Scanning the AIA data, we also find that the type of event presented in this paper is commonplace. This finding suggests that interchange/slipping reconnection processes may occur frequently in the pre-disposed S-Web

environment, and according to our results, relies on gradual interchange/slipping reconnection. Such solar phenomena may continuously release a significant amount of mass and energy into the heliosphere (van Driel-Gesztelyi et al. 2012) and therefore may play a critical role in the wind generation.

## REFERENCES

Altschuler, M. D., & Newkirk, G. 1969, SoPh, 9, 131
Antiochos, S. K., Karpen, J. T., & DeVore, C. R. 2002, ApJ, 575, 578
Antiochos, S. K., Linker, J. A., Lionello, R., et al. 2012, SSRv, 172, 169
Antiochos, S. K., Mikić, Z., Titov, V. S., Lionello, R., & Linker, J. A. 2011, ApJ, 731, 112
Aulanier, G., Golub, L., DeLuca, E. E., et al. 2007, Sci, 318, 1588
Aulanier, G., Pariat, E., Démoulin, P., & Devore, C. R. 2006, SoPh, 238, 347
Aulanier, G., Török, T., Démoulin, P., & DeLuca, E. E. 2010, ApJ, 708, 314
Baker, D., van Driel-Gesztelyi, L., Mandrini, C. H., Démoulin, P., & Murray, M. J. 2009, ApJ, 705, 926
Bradshaw, S. J., Aulanier, G., & Del Zanna, G. 2011, ApJ, 743, 66
Brown, D. S., & Priest, E. R. 2001, A&A, 367, 339
Cirtain, J. W., Golub, L., Lundquist, L., et al. 2007, Sci, 318, 1580
Delannée, C., Török, T., Aulanier, G., & Hochedez, J.-F. 2008, SoPh, 247, 123
Démoulin, P. 2006, AdSpR, 37, 1269
Démoulin, P., Mandrini, C. H., Rovira, M. G., Henoux, J. C., & Machado, M. E. 1994, SoPh, 150, 221
Del Zanna, G. 2008, A&A, 481, L49
Edmondson, J. K., Antiochos, S. K., DeVore, C. R., Lynch, B. J., & Zurbuchen, T. H. 2010, ApJ, 714, 517
Edmondson, J. K., Lynch, B. J., Antiochos, S. K., De Vore, C. R., & Zurbuchen, T. H. 2009, ApJ, 707, 1427
Filippov, B., Koutchmy, S., & Tavabi, E. 2013, SoPh, 286, 143
Galsgaard, K., & Pontin, D. I. 2011, A&A, 534, A2
Galsgaard, K., Priest, E. R., & Titov, V. S. 2003, JGR, 108, 1042
Habbal, S. R., Druckmüller, M., Morgan, H., et al. 2011, ApJ, 734, 120
Lemen, J. R., Title, A. M., Akin, D. J., et al. 2012, SoPh, 275, 17
Linker, J. A., Lionello, R., Mikić, Z., Titov, V. S., & Antiochos, S. K. 2011, ApJ, 731, 110
Mandrini, C. H., Démoulin, P., Bagala, L. G., et al. 1997, SoPh, 174, 229
Masson, S., Aulanier, G., Pariat, E., & Klein, K.-L. 2012, SoPh, 276, 199
Masson, S., Pariat, E., Aulanier, G., & Schrijver, C. J. 2009, ApJ, 700, 559
Moreno-Insertis, F., Galsgaard, K., & Ugarte-Urra, I. 2008, ApJL, 673, L211
O'Dwyer, B., Del Zanna, G., Mason, H. E., Weber, M. A., & Tripathi, D. 2010, A&A, 521, A21
Pariat, E., Antiochos, S. K., & DeVore, C. R. 2009, ApJ, 691, 61
Parnell, C. E., Haynes, A. L., & Galsgaard, K. 2010, JGRA, 115, 2102
Pesnell, W. D., Thompson, B. J., & Chamberlin, P. C. 2012, SoPh, 275, 3
Priest, E. R., & Démoulin, P. 1995, JGR, 100, 23443
Priest, E. R., Hornig, G., & Pontin, D. I. 2003, JGR, 108, 1285
Reeves, K. K., Linker, J. A., Mikić, Z., & Forbes, T. G. 2010, ApJ, 721, 1547
Reeves, K. K., Warren, H. P., & Forbes, T. G. 2007, ApJ, 668, 1210
Reid, H. A. S., Vilmer, N., Aulanier, G., & Pariat, E. 2012, A&A, 547, A52
Rickard, G. J., & Titov, V. S. 1996, ApJ, 472, 840
Savcheva, A., Pariat, E., van Ballegooijen, A., Aulanier, G., & DeLuca, E. 2012, ApJ, 750, 15
Schou, J., Scherrer, P. H., Bush, R. I., et al. 2012, SoPh, 275, 229
Schrijver, C. J., & De Rosa, M. L. 2003, SoPh, 212, 165
Seaton, D. B., De Groof, A., Shearer, P., Berghmans, D., & Nicula, B. 2013, ApJ, 777, 72
Sheeley, N. R., Jr., Wang, Y.-M., Hawley, S. H., et al. 1997, ApJ, 484, 472
Sun, X., Hoeksema, J. T., Liu, Y., et al. 2013, ApJ, 778, 139
Titov, V. S., Mikić, Z., Linker, J. A., Lionello, R., & Antiochos, S. K. 2011, ApJ, 731, 111

Titov, V. S., Mikic, Z., Török, T., Linker, J. A., & Panasenco, O. 2012, ApJ, 759, 70

van Driel-Gesztelyi, L., Culhane, J. L., Baker, D., et al. 2012, SoPh, 228, 237

Wang, Y., Biersteker, J. B., Sheeley, N. R., Jr., et al. 2007, ApJ, 660, 882

Wang, Y.-M., Grappin, R., Robbrecht, E., & Sheeley, N. R., Jr. 2012, ApJ, 749, 182

Wang, Y.-M., Sheeley, N. R., Socker, D. G., Howard, R. A., & Rich, N. B. 2000, JGR, 105, 25133

Wang, Y.-M., Sheeley, N. R., Jr., Walters, J. H., et al. 1998, ApJL, 498, L165

Zurbuchen, T. H., Fisk, L. A., Gloeckler, G., & von Steiger, R. 2002, GeoRL, 29, 1352